Robust Small Signal Stability for Microgrids under Uncertainty

Jorge Elizondo, Richard Y. Zhang, Jacob K. White, and James L. Kirtley Jr.
Department of Electrical Engineering & Computer Science
Massachusetts Institute of Technology
Cambridge, MA 02139, USA
{jelizon, ryz, white, kirtley}@mit.edu

***Abstract*—We describe an adapted robust control technique for analyzing microgrid stability under the uncertainty of renewable sources and loads. Two realistic case studies are presented to demonstrate the method's effectiveness as a tool for system design and analysis. Results show that the method is able to provide a non-trivial lower bound for the minimum damping ratio of the system, and can find the unstable instances missed by Monte Carlo approaches.**

I. Introduction

The integration of renewable energy sources may significantly complicate power system stability. Their short-time variations introduce persistent, small-signal disturbances on the network; the uncertainty in their long-term power production increases the dynamic range of network states.

Stability issues are particularly significant for microgrids, which are smaller–both physically and in power rating– when compared to conventional distribution networks. Microgrids have lower inertia and tighter coupling between elements, so integration of renewables can make stability problems more likely to occur. Moreover, microgrids frequently undergo topological changes, due to routine opening and closing of switches, as well as the addition of new sources and loads, even after controls have been set-up and the system is operational.

Under typical conditions, disturbances caused by the variability of renewables are small enough to be analyzed using linearization, a procedure known as *small-signal analysis* [1], [2]. Loosely speaking, this involves computing the damping ratio of the system's linearization, ζ, and insuring that the damping ratio exceeds a given threshold. When subject to uncertainty in the system, small-signal stability analysis is required for *all feasible uncertain scenarios*, a computationally daunting task. For example, with solar irradiance being uncertain and unknown, the system should remain stable for all combinations of solar panel outputs, from zero up to the maximum for each individual panel.

By applying robust control techniques, this paper proposes to *provably guarantee* small-signal stability for microgrids under the uncertainty of renewables and loads. The method works by establishing a lower-bound for the *minimum* damping ratio, which is defined as the damping ratio of the least-stable feasible scenario. Clearly, if the lower bound is shown to be acceptable, then the worst-case, least-stable scenario must still be stable, and it immediately follows that all other uncertain scenarios are also stable.

The robust approach contrasts with most existing methods for analyzing small-signal stability under uncertainty, all sharing a common probabilistic theme. The basic Monte Carlo method works by analyzing the statistics for randomly selected uncertain scenarios. Its efficiency can be enhanced by quasi-random sampling, moment matching, collocation [3], [4] and incorporating sensitivities [5], [6]. While probabilistic methods are highly effective at analyzing the average-case, they are ineffective at probing the worst-case.

The idea of analyzing power systems using techniques borrowed from robust controls reappeared frequently in the literature, particularly after the development of efficient primal-dual interior point methods [7]–[11]. Despite this, robust methods have yet to become widespread. A significant reason is that their computation complexity, on the order of $O(n^4)$, still grows too quickly for traditional power systems, which contain thousands of elements, i.e. with $n \gg 10^3$. But microgrids are significantly smaller, of sizes comparable to the (larger) control systems commonly studied in robust control. With the development of high-power, commercial-grade solvers [12], and increasingly inexpensive access to massive computation power, semidefinite optimization is becoming a viable tool for power systems stability analysis [13], [14].

To compare the proposed approach and traditional methods, we present two case studies that represent simple but realistic scenarios. The starting point for both consists of a simple two-bus system with a single machine and a single load connected through a transmission line. In Case Study 1, we consider the scenario of expanding the system by interconnecting solar photovoltaic (PV) panels somewhere along the transmission line. This scenario is encountered frequently in new or existing off-grid microgrids that wish to minimize fuel consumption. Case Study 2 expands the system even further by adding a second machine, incorporating two extra loads buses and changing the network to allow for a ring topology. The resultant system represents a variety of realistic scenarios, such as a small community isolated from the grid, or a university campus that is temporarily disconnected from the utility.

II. Theoretical Background

A. Small signal stability

Consider a state-space model[1] of a power system

$$\dot{x}(t) = f(x(t)) + w(t) \qquad x(0) = x_0, \tag{1}$$

[1]In practice, power systems are modeled as differential algebraic systems. Extension to differential algebraic equations are straightforward, via singular perturbations and / or descriptor state-space formulations; see [15], [16]. For brevity, these extensions are omitted in this paper.

978-1-4799-8586-9/15/$31.00 (c)2015 IEEE

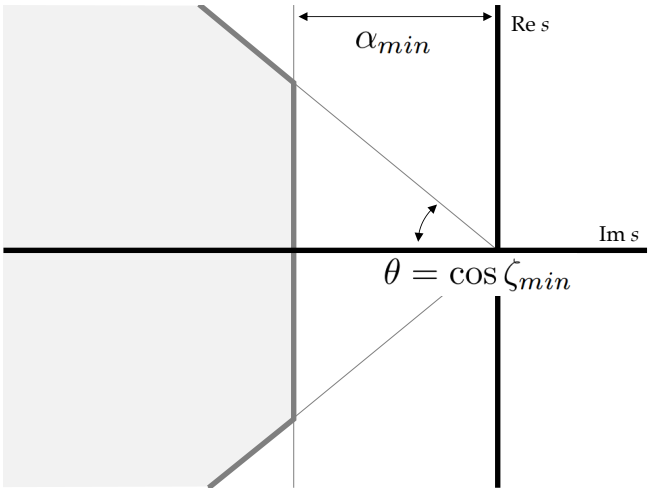

Figure 1: Small-signal stability on the complex plane. Every eigenvalue $\lambda_k = -\alpha_k + j\omega_k$ placed in the shaded region will satisfy the decay rate constraint $\alpha_k \geq \alpha_{min}$ and the decay ratio constraint $\alpha_k/|\lambda_k| \geq \zeta_{min}$.

where $x(t) \in \mathbb{R}^n$ is the vector of state variables and $w(t) \in \mathbb{R}^n$ represents the disturbances on the system. The system is in equilibrium $x(0) = x_0$ when it satisfies

$$f(x_0) = 0, \tag{2}$$

so that without disturbance, i.e. by setting $w(t) = 0$, the system would remain fixed at $x(t) = x_0$ for all time.

Define $A := \nabla_x f(x_0)$ as the Jacobian matrix of $f(\cdot)$ evaluated at the equilibrium x_0. Then the stability of (1) about its equilibrium is captured by the linear time-invariant system

$$\dot{x}(t) = Ax(t) + w(t). \tag{3}$$

Two common metrics of stability are the *damping ratio*,

$$\zeta \triangleq \min_k\{-\mathrm{Re}\,\lambda_k/|\lambda_k|\}, \tag{4}$$

and the *decay rate*,

$$\alpha \triangleq \min_k\{-\mathrm{Re}\,\lambda_k\}, \tag{5}$$

in which we have labeled the k-th eigenvalue of A as λ_k.

Using these definitions, a power system is said to be *small-signal stable* (about its equilibrium x_0) if its decay rate and damping ratio satisfy certain thresholds:

$$\zeta \geq \zeta_{lim} \qquad \alpha \geq \alpha_{lim}. \tag{6}$$

For large power networks, minimum damping ratios are usually specified to exceed 3% to 5%. Low-frequency oscillations may be required to have damping ratios as high as 15% [9]. In comparison, minimum decay rate specifications are more commonly found in the design of control systems.

From a control theory perspective, these stability criteria form a trapezoidal envelope on the complex plane, as shown in Fig. 1. In order for A to be deemed "sufficiently stable", all of its eigenvalues must lie within this envelope. Clearly, both ζ and α must be strictly positive if a system were to be stable.

B. Parametric uncertainty

It is often convenient to describe uncertain systems as deterministic with respect to uncertain parameters. In the context of the power system equations in (1), an l-dimensional parameter variable, q, may be added, as in

$$\dot{x}(t) = f(x(t), q) + w(t), \qquad x(0) = x_0(q), \tag{7}$$

so that every value of q, constrained within a parameter space $\mathcal{Q} \in \mathbb{R}^l$, is associated with an uncertain scenario to be considered and analyzed. To illustrate, a system containing l solar panels may define q to capture the uncertainty of solar irradiance. In this case, each $q_1, q_2, \ldots, q_l$ can be used to describe the power output at solar panel, and $\mathcal{Q}$ to constrain each output to lie between zero and its maximum.

Every uncertain scenario, q, also has its own steady-state, $x_0(q)$, and Jacobian matrix evaluated at that steady-state, $A(q) := \nabla f_x(x_0(q), q)$. From this, a linearized dynamical system is defined for each value of q, as in

$$\dot{x}(t) = A(q)x(t) + w(t). \tag{8}$$

Just like in (3), the stability characteristics of (8) are captured by the matrix $A(q)$.

Let us define the $\zeta(\cdot)$, $\alpha(\cdot)$ functions to yield the damping ratio and decay rate of a given matrix, and Ω be the space of all Jacobian matrices obtainable under uncertainty

$$\Omega = \{A(q) : q \in \mathcal{Q}\}. \tag{9}$$

Analogous to the criteria in (6), if the minimum damping ratio (ζ_{min}) and the minimum decay rate (α_{min}) defined as

$$\zeta_{min} \triangleq \min\{\zeta(A(q)) : q \in \mathcal{Q}\}, \tag{10}$$

$$\alpha_{min} \triangleq \min\{\alpha(A(q)) : q \in \mathcal{Q}\}, \tag{11}$$

both satisfy $\zeta_{min} \geq \zeta_{lim}$ and $\alpha_{min} \geq \alpha_{lim}$, then every uncertain scenario must be small-signal stable. In this case, we say that $\mathcal{Q}$ is stable (for brevity).

C. Robust stability lower-bounds via LMIs

When Ω, defined in (9), satisfies certain conditions, lower-bounds for ζ_{min} and α_{min} can be computed by solving convex optimization problems known as linear matrix inequalities (LMIs). In particular, this is possible when Ω is a polytope, i.e., when Ω can be written as the convex hull of m "vertex" matrices, $A_1, \ldots, A_m$

$$\Omega = \mathrm{conv}\{A_1, A_2, \ldots, A_m\}.$$

Given a matrix polytope, Ω, the following statements[2] are well-known [9], [17].

Proposition 1 (Minimum decay rate)**.** *Every matrix in the polytope Ω has a decay rate that exceeds the lower-bound α_{lb}, defined as the solution to the optimization problem*

$$\begin{aligned} &\textit{maximize} && \alpha \\ &\textit{subject to} && A_i^T X + X A_i + 2\alpha X \preceq 0 \quad \forall i, \\ & && X = X^T \succeq I. \end{aligned}$$

Proposition 2 (Minimum damping ratio)**.** *Every matrix in the polytope Ω has a damping ratio that exceeds the*

[2]We use standard notation in matrix optimization. Given symmetric matrices X, Y, we say that $X \succeq Y$ iff the matrix $X - Y$ is positive semidefinite (i.e. its eigenvalues are nonnegative).

lower-bound ζ_{lb}, defined as the solution to the optimization problem

$$\begin{aligned} &\textit{maximize} && \zeta \\ &\textit{subject to} && \begin{bmatrix} \nu(A_i^T X + X A_i) & \zeta(A_i^T X - X A_i) \\ \zeta(A_i X - X A_i^T) & \nu(A_i^T X + X A_i) \end{bmatrix} \preceq 0 \quad \forall i, \\ & && 0 \leq \zeta, \nu \leq 1 \qquad \nu^2 + \zeta^2 = 1, \\ & && X = X^T \succeq I. \end{aligned}$$

Both optimization problems in Props. 1 & 2 are quasi-convex, and can be efficiently solved using any semidefinite programming solver. In this paper, the problems are parsed using the YALMIP package [18], and solved using MOSEK [12].

In practice, Ω is not usually a matrix polytope, and it is often necessary to construct an outer approximation $\Omega_{out} \supseteq \Omega$. This can be achieved in many ways. In this paper, we use the state-space sampling approach of [19], and the inclusion $\Omega_{out} \supseteq \Omega$ is guaranteed by *a priori* knowledge of the Lipschitz constants associated with the $A(q)$ operator in (9). Other techniques include Lur'e-type sector conditions [13], polynomial-based linear matrix inequalities [20], [21], and sum-of-squares programming [22].

We conclude this section by noting that robust stability is inherently pessimistic. Since $\zeta_{lb} \leq \zeta_{min}$ and $\alpha_{lb} \leq \alpha_{min}$, it is possible for both ζ_{lb}, α_{lb} to indicate instability when every uncertain scenario is in fact stable. This conservatism arises for two reasons:

1) Quadratic stability. Both Props. 1 & 2 constraints, based on quadratic stability, are sufficient but not always necessary conditions for stability [23].
2) Outer approximation. If the Ω_{out} in Props. 1 & 2 is larger than Ω, then it is possible for the least stable element of Ω_{out} to be outside of Ω. In other words, the least-stable element found may not actually be realizable.

Although it dramatically increased computation cost, both sources of conservatism were reduced by dividing Ω into partitions and employing a branch-and-bound process [7], [24], [25].

III. Microgrid Models

The example microgrid systems considered in this paper are constructed with four elements:

1) Diesel generators that interface with the network through a synchronous machine;
2) Solar PV panels that connect to the system through inverters;
3) Constant-impedance loads modeled as parallel resistor-inductor tanks;
4) Transmission lines modeled as series resistor-inductor branches.

A multitude of microgrid systems can be built using these four elements as both sources with and without inertia are represented, and it incorporates loads with a variety of power factors. Extending the model to include other types of sources (such as gas-turbine generators) and other types of static and dynamic loads is possible with this formalism, but it is left as future work.

A. Diesel Generator

The diesel generator sources were modeled in detail and included the following blocks:

1) Synchronous machine with mechanical, armature, field and damper dynamics;
2) Diesel engine and governor (speed controller);
3) Automatic voltage regulator (AVR) with exciter and power system stabilizer (PSS).

All these blocks are required for a complete small-signal representation of this source [26]. Power-frequency (PF) droops and line compensators for real and reactive power sharing were accounted for in the power flow calculations used to determine the steady state operation of the system. Limits on the prime mover output torque, exciter output voltage, secondary control and protective elements were not included in the model as they do not affect the small-signal behavior.

To obtain significant results, realistic parameters for the synchronous machine, and appropriate models for the diesel engine and the AVR are needed; they all can have a significant impact on system small-signal dynamics. For that, machine parameters were taken from technical specifications of a commercial generator manufacturer [27], and the AVR and exciter models were taken from IEEE Std. 421.5 [28]. Type DC1A exciter was chosen as it has been widely used in industry.

The models for prime movers have not been standardized and several representations can be found in literature. We selected the diesel engine model presented in [29] that was shown to match experimental data; this model has also been used in [30] for stability studies. The parameters in [29] were given for a 0.85 MVA engine and we had to scale them down to the rating of the machines in our systems. A linear relationship between the engine time constant and power rating was assumed.

B. Solar Photovoltaic Panels

The solar PV panels and inverter were modeled with three main blocks following studies such as [31]:

1) A filter, consisting of an inductor and its parasitic resistance;
2) Inner current control loops;
3) Outer control loops.

The filter inductor was set to a value of 1mH which was found to properly filter the inverter current ripple at 20kHz caused by switching. The inner current control loops were design for a critically damped response. The inverter was operated in "Slave" (or "Grid-following") mode with a Phase Locked Loop (PLL) used to synchronize it to the system. We assumed that PLLs track phase and correct small errors almost instantaneously and therefore PLL dynamics were ignored in the small-signal model. An average model of the converter was used so that the switch bridge characteristics and delays were also ignored.

With the outer control loop, inverters were operated in three different modes: (a) Unitity power factor, (b) Voltage support (i.e. using QV droops), and (c) Voltage regulation (i.e. operation as a P-V bus). For the last two cases, after the inverter power rating was reached, priority was given to real power output. The inverter real power output was assumed to follow changes in solar irradiation instantaneously and

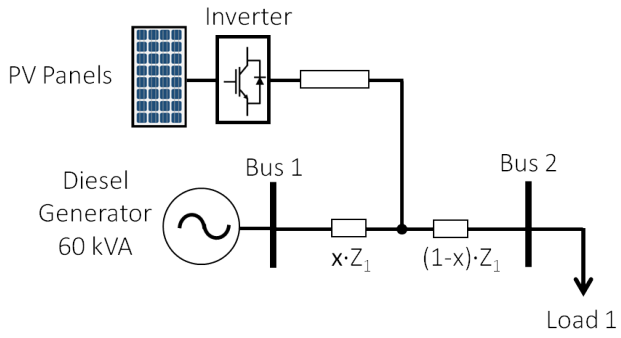

Figure 2: Single line layout of system for Case Study 1

therefore DC link and maximum power point tracker dynamics were not included in the small signal model.

C. Network interconnection

In large power systems, transmission line dynamics are usually assumed to be instantaneous. That is reasonable if both the frequency and voltage control loops are several orders of magnitude slower than the line time constant. In microgrids, however, the presence of inverter-interfaced sources, the fast acting AVR in the machines, and the low inertia, combine to create strong coupling between the line and the element states.

Accounting for the network, the system model becomes a set of differential-algebraic equations (DAEs),

$$\frac{\mathrm{d}}{\mathrm{d}t}x = f(x,y), \qquad 0 = g(x,y), \tag{12}$$

where $x \in \mathbb{R}^n$ are the states of the system (e.g. machines fluxes, rotor angles and velocities, inverter filter currents, etc), and $y \in \mathbb{R}^m$ are the algebraic variables (bus voltages). As mentioned above, the theoretical background presented in Section II can be extended to DAEs.

IV. Case Study 1: Interconnection of PV Panels to a Two-Bus System

Two case studies are given below and used to compare the proposed robust approach to the traditional stochastic method. The system for the first case study is constructed starting with a simple two-bus system where a diesel generator feeds a single load through a transmission line, and then PV panels are interconnected somewhere along the line as illustrated in Fig. 2. From a design point of view, we want to (a) guarantee that the system will be stable after the insertion of the panels and (b) quantify the impact that the panels will have on the system stability.

The diesel generator in Fig. 2 is a 60kVA 480V 1800 rpm machine, and the transmission line is specified to be of 1 km in length, with a resistance of 0.1Ω and an inductance of 66 μH. The generator is operated in isochronous mode, i.e. with its PF droop coefficient set to zero. Its control system (exciter, governor, PSS) was designed prior to the insertion of the solar panels and was set to achieve an approximate damping ratio of ~15% at high load and low power factor.

Three sources of uncertainty are considered:

1) PV panels insertion point, labeled x in Fig. 2. The value of $x = 0$ corresponds to connecting the panels right next to the generator terminals, while $x = 1$ represents a connection at the load.

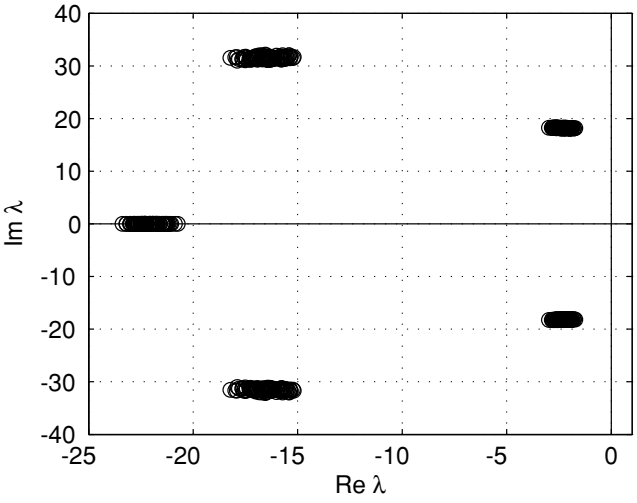

(a)

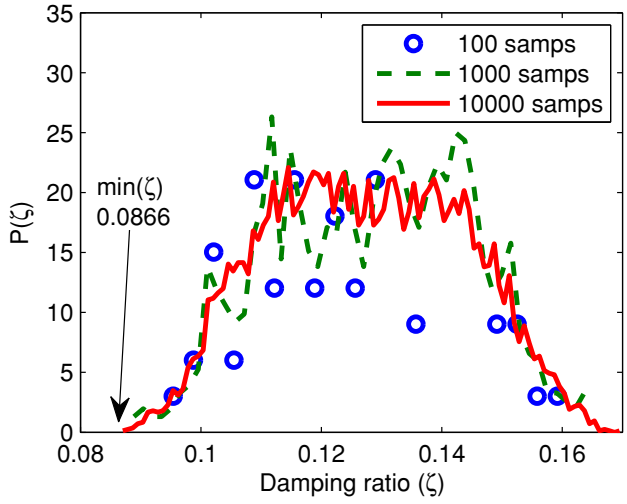

(b)

Figure 3: Monte Carlo analysis for $l = 1$ km and $^{X}/_{R} = 0.25$, sampled over all possible values of $\{x, S_{load}, \phi_{load}, P_{inv}\}$: (a) Complex plane eigenvalue plot over 100 samples; (b) decay ratio (ζ) histogram; minimum over 10,000 samples is $\zeta = 0.086$.

2) Load in kVA, labeled S_{load}, and power angle, labeled ϕ_{load}. The load is modeled to be residential, ranging from 40-60 kVA with a power angle from 0° to 15° (i.e. power factors from about 0.95 to 1.00).
3) Real power output of solar panels, labeled P_{inv}, whose value ranges between 0 kW during the night and 30 kW at peak day-time irradiance. This way, the peak renewable penetration achievable is 50%.

A. Monte Carlo Analysis

Monte Carlo and, in general, any stochastic method provides optimistic over-estimates for the minimum damping ratio (ζ_{ub}) and for the minimum decay rate of the system (α_{ub}). However, they are unable to guarantee that the worst-case condition has been found or even provide a certificate of stability. Results for Case Study 1 are shown in Fig. 3. The value of ζ for every instance of the system was computed relatively fast, but, as seen in Fig. 3, 10,000 samples were needed to find the value of $\zeta_{ub} = 8.6\%$. Furthermore, as the number of uncertain parameters increases,

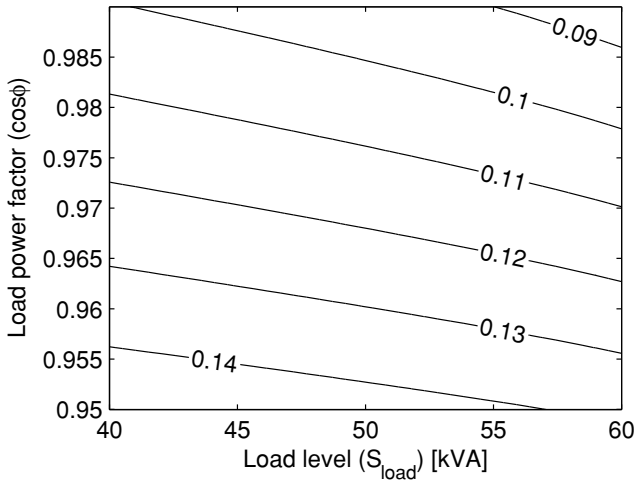

Figure 4: Contour plot of damping ratio ζ with PV panels inserted at generator ($x = 0$) and providing only reactive power support ($P_{inv} = 0$).

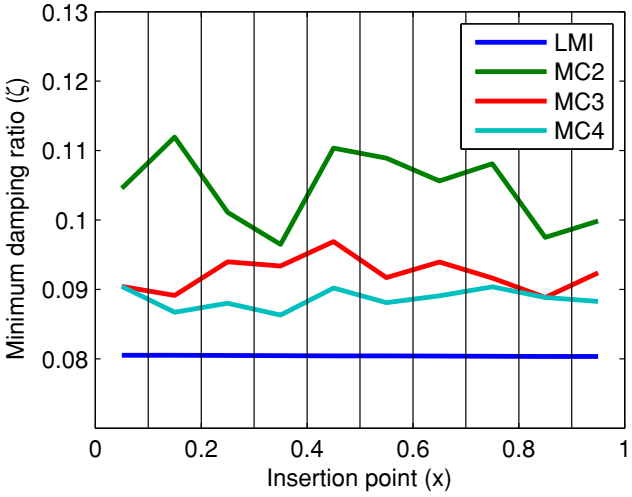

(a)

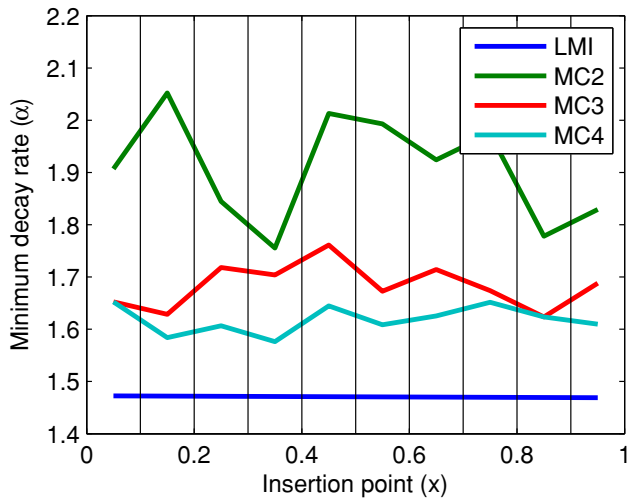

(b)

Figure 5: Minimum damping ratios across all uncertainty in system 1.

the required number of samples to find an upper bound that provides valuable information increases as well.

B. Robust lower bounds

While the stochastic analysis provided optimistic over-estimates (ζ_{ub} and α_{ub}), the robust method presented in Section II-C is able to calculate pessimistic under-estimates of the same variables (ζ_{lb} and α_{lb}). In this application, lower bounds are useful because they can guarantee that the system will be stable under any conditions. By solving the LMIs, we found the lower bounds $\zeta_{lb} = 8\%$ and $\alpha_{lb} = 1.48$. Note that these lower bounds are (mildly) more conservative than necessary, due to the need to form an outer approximation (see Section II-C). The number of states in the system is sufficiently low ($n = 27$), and the LMIs in Section II-C computed each bound in ~200 seconds on a 12-core machine running MOSEK 7.1.0.12 [12].

C. Results and Discussion

By using the proposed robust method, it was possible to compute the value of $q = [x, S_{load}, \phi_{load}, P_{inv}]$ that resulted in the instance of the system with minimum damping ratio. We found that connecting the PV as close as possible to the generator ($x = 0$) , providing only reactive power ($P_{inv} = 0$), and operating at maximum load ($S_{load} = 60$kVA) with unity power factor ($\cos\phi = 1$) resulted in the least damped system. The described system correspond to the condition where the generator is loaded the most, and has a damping ratio of at least $\zeta_{lb} = 8\%$. Figure 4 shows a contour plot of ζ for the allowed values of S_{load} and $\cos\phi$. Notice that for this system, the worst-case condition is located at a corner of the parameter space $\mathcal{Q}$, which means that all unknown variables take a value at the limit of their range. This will not be true in general (see Case Study 2), and using the simple heuristic of testing the corner values of the parameter space to find the least-stable system might lead to incorrect results.

A graphical comparison of the results obtained with the traditional Monte Carlo approach and the robust method is shown in Fig. 5, for different points of PV panel insertion. In these plots we can clearly appreciate the advantage of providing a lower bound for the minimum damping ratio. While the Monte Carlo results establish that the actual minimum damping ratio will be *below* its corresponding line, the robust result guarantees that the actual value will be *above* it. This means that the robust method can provide a certificate of stability, while the Monte Carlo results only indicate that the system is likely to be stable.

In this case study, the least-stable eigenvalues of the system were associated with the mechanical modes of the system. This was expected, as the inertia time constant of the machines and engines is longer than the electrical time constants of the system. This result, however, is not general and changing the diesel generator parameters will lead to different results. An exploration of the complex plane eigenvalue plot of the system also revealed that, for the chosen parameters, the largest impact of the PV panels is caused by their effect on the operational equilibrium point x_0. The inverter states have a small effect on the least damped mode, so that it is possible to apply a model order reduction technique before solving for the LMI. This route seems promising as a way to extend this methodology and will be explored in future work.

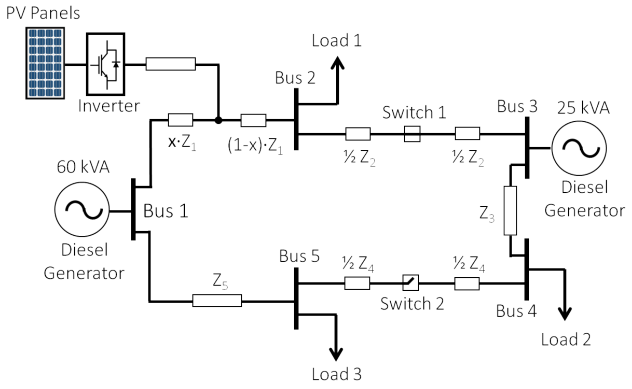

Figure 6: Single line layout of system for Case Study 2

V. Case Study 2: Interconnection of PV in a Two-Machine System

The presence of uncertainty in power systems will often lead to unintuitive results, which cannot be found using simple heuristics. Although in Case Study 1 the least stable condition was found to be at a corner of the parameter space, this will not be true in general. In the Case Study 2, we consider the larger two-machine five-bus system shown in Fig. 6. As with the first system, it was built from a simple two-bus system so that the control parameters of the 60 kVA machine were not changed as new elements were being added (except for adding a non-zero droop coefficient). The second diesel generator is a 25kVA 480V 1800 rpm machine, and the distance between all elements is assumed to be constant at 1 km, so that transmission line parameters are the same as in Case Study 1.

Several characteristics make this system interesting and relevant for uncertainty studies:

1) Power is supplied by two generators sharing real power and interaction between them is expected.
2) The control parameters of the larger generator are not modified from Case Study 1 because the new system is assumed to be built after the first.
3) The network can operate in a radial or a ring topology, so that power flow can change significantly with the operation of the switches.
4) As it is sometimes the case in real scenarios, the maximum and minimum total load is known, but its distribution among the different load buses is not.

Five sources of uncertainty are considered in this case study:

1) Inverter insertion point. The branch at which the inverter is connected is described by an integer variable and the position within that branch is described by a continuous variable $x \in [0, 1]$ as per Case Study 1.
2) The status of the two switches, which are determined by two binary variables.
3) Total load in kVA, labeled S_{load}, and power angle, labeled ϕ_{load}. This value ranges from 30 kVA to 85 kVA, and represents the addition of the three load buses shown in Fig. 6.
4) The share of the total load connected to each load bus, represented by three variables $k_1, k_2, k_3 \in [0, 1]$ satisfying $k_1 + k_2 + k_3 = 1$.
5) PV panels real power output, labeled P_{inv}, whose value ranges from 0 kW during the night to 30 kW at peak day-time irradiance.

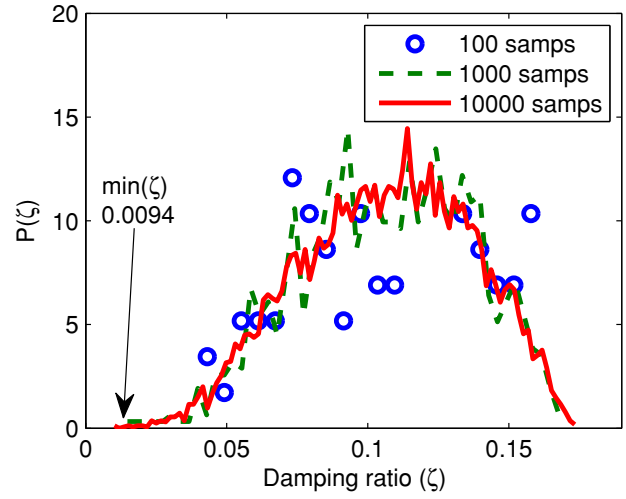

(a)

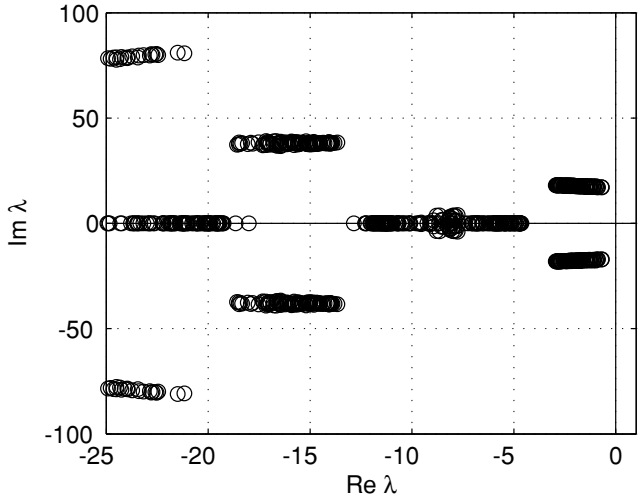

(b)

Figure 7: Monte Carlo analysis for switch 1 open and switch 2 closed: (a) Complex plane eigenvalue plot over 100 random samples

A. Monte Carlo Analysis

As with the previous case study, the Monte Carlo method was used to determine an optimistic over-estimate for the minimum damping ratio (ζ_{ub}). Fig. 7a shows an histogram of the obtained values of ζ_{lb} for the configuration with switch 1 open and switch 2 closed. It can be observed that in the vast majority of the conditions the system exhibits a reasonable level of damping ($\zeta \geq 3\%$ in 99.6% of the 10,000 random samples), but certain configurations can take the system below the desired threshold. After sampling 10,000 conditions, we found the minimum damping ratio to have an upper bound of $\zeta_{ub} = 0.94\%$. Fig. 7b shows the eigenvalue distribution on the complex plane after 100 random samples. Note that the rightmost eigenvalue is dangerously close to the imaginary axis, but remains on the left-half plane.

Table I: Stability over-estimates via Monte Carlo ("MC") over 100, 1000 and 10,000 samples and under-estimates via linear matrix inequalities ("LMI").

Minimum damping ratio (ζ) over uncertainty in percentage [%]

SW1	SW2	MC (10^2)	MC (10^3)	MC (10^4)	LMI
closed	open	4.00	1.32	0.94	unstable
closed	closed	1.97	1.97	0.51	unstable
open	closed	3.64	2.22	unstable	unstable

Minimum decay rate (α) over uncertainty in per-seconds [s^{-1}]

SW1	SW2	MC (10^2)	MC (10^3)	MC (10^4)	LMI
closed	open	0.684	0.231	0.162	-0.4
closed	closed	0.340	0.340	0.086	-0.4
open	closed	0.639	0.390	-0.047	-0.4

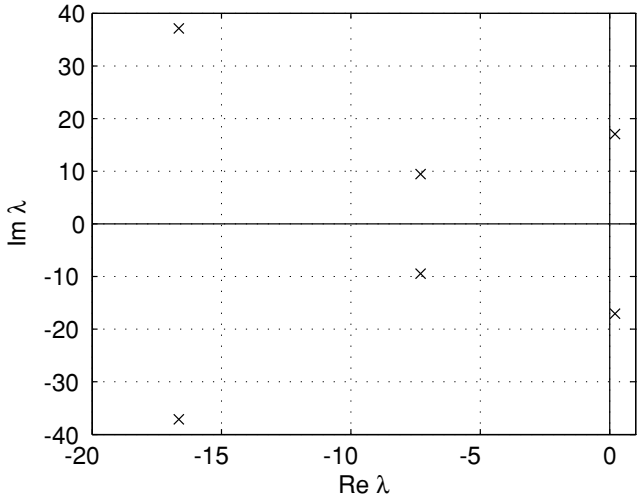

Figure 8: Eigenvalue plot for an unstable system found via the LMI method. The instance of the system corresponds to connecting the PV panels in branch 1 at $x = 0.99$ (next to Bus 2) with switch 1 closed and switch 2 open. Load was close to its maximum ($S_{load} = 84.9$ kVA) and power factor near unity ($\cos\phi = 0.99$). Distributed over the three buses was as follows: $k_1 = 0.81$, $k_2 = 0.01$, $k_3 = 0.18$. This particular case has decay rate $\alpha \approx -0.2$ and damping ratio $\zeta \approx -1\%$.

B. Robust analysis

The robust method was used to compute the lower bounds ζ_{lb} and α_{lb}. Interestingly, we found the lower bounds to be unstable in all configurations of the switches. Having an unstable lower bound means that the system might be unstable. In this case, however, we were able to use the least stable parameters q found by the the robust analysis to prove that the system is unstable. It is worth noticing that due to the size of this system ($n = 77$) solving the LMI required several days of computation, so extending this method to larger systems will require a model order reduction technique and an application-specific LMI solver, such as those in [32], [33].

C. Results and Discussion

As mentioned above, some instances of the system were found to be unstable. From Fig. 7a we know that they represent a small minority of all the possible scenarios, but improper system design and bad luck can lead to such conditions. Table I presents the over-estimates (ζ_{ub} and α_{ub}) using Monte Carlo and the under-estimates (ζ_{lb} and α_{lb}) using LMIs for the three valid configurations of the switches. Notice that Monte Carlo was able to find an unstable condition in one of the 10,000 sampled scenarios. The possibility of finding such cases is low, as they occur far from the mean of the probability density function for ζ. In the cases were Monte Carlo provided stable over-estimates (ζ_{ub} and α_{ub}) and instability was not guaranteed, the system was proved to be unstable by calculating the eigenvalues of the worst-case instance found by the LMIs.

An example of an unstable instance of the system found by the LMI method is shown in Fig. 8. This unstable scenario corresponds to maximum load ($S_{load} = 84.9$ kVA) and near unity power factor ($\cos\phi = 0.99$), with PV panels providing a low value of real power output ($P_{inv} = 80$W) but providing a large amount of reactive power to regulate its terminal voltage (i.e. it was operated in voltage regulation mode). The position for the inverters is next to Bus 2 where more than 80% of the total load is connected; the rest of the load is connected in Bus 5, leaving Bus 4 only very lightly loaded. The above conditions require the generators to operate near unity power factor (as most reactive power is provided by the inverter) and heavily loaded, which leads to small signal instability. We emphasize that the unstable scenario was not found at a corner of the parameter space $\mathcal{Q}$; conversely, checking only the corners of $\mathcal{Q}$ would not have revealed the instability.

The instability in this Case Study can be explained by three factors: (a) Improper control parameters for the large 60 kVA diesel generator, (b) operation of the inverter as a P-V bus, and (c) high penetration of renewables that leads to a large inverter connected in the system. As explained above, this system was constructed starting from a simple two-bus system with a 60 kVA diesel generator feeding a single load. The system was then expanded to include a second machine and other loads, but control parameters for the original machine remained unchanged. This process mimics the way real-life microgrids are sometimes built and expanded; one presumes that the system can be made stable by properly adjusting the control parameters of the large diesel generator, under the conditions that lead to Fig. 8. On the other hand, inverter control via voltage regulation (i.e. behaving as a P-V bus) often created the largest disturbance in the system, especially when connected close to the largest load and with low real power output as more of the inverter power rating could be dedicated to reactive power. It is worth mentioning that the scenario corresponding to Fig. 8 was not unstable when the inverter was operated at unity power factor or just providing voltage support with a droop of 1000 VAr/V.

VI. Conclusions

The Monte Carlo technique and our robust stability method based on LMIs were applied to two case studies of microgrids with uncertainty due to renewable sources and loads. The ability of robust stability methods to generate provable lower bounds is shown to be a valuable tool during system design and analysis of microgrids. Our approach either guaranteed stability (such as Case Study 1) under any condition, or uncovered instability in a few instances missed by Monte Carlo (such as Case Study 2). Although the functionality and usefulness of the robust stability technique was demonstrated, it required a large computational effort given

the system had only 77 states. Therefore, the next steps will be to implement model order reduction to eliminate unnecessary states, and to use more efficient solvers for the LMIs.

VII. Acknowledgments

Financial support for this work was provided by the Cooperative Agreement between the Masdar Institute of Science and Technology (Masdar Institute), Abu Dhabi, UAE and the Massachusetts Institute of Technology (MIT), Cambridge, MA, USA (Reference 02/MI/MI/CP/11/07633/GEN/G/00), the MIT Energy Initiative and the Skolkovo-MIT Initiative in Computational Mathematics.

References

[1] S. Eftekharnejad, V. Vittal, G. T. Heydt, B. Keel, and J. Loehr, "Small signal stability assessment of power systems with increased penetration of photovoltaic generation: A case study," *Sustainable Energy, IEEE Transactions on*, vol. 4, no. 4, pp. 960–967, 2013.

[2] R. Shah, N. Mithulananthan, R. Bansal, and V. Ramachandaramurthy, "A review of key power system stability challenges for large-scale pv integration," *Renewable and Sustainable Energy Reviews*, vol. 41, pp. 1423–1436, 2015.

[3] J. L. Rueda, D. G. Colomé, and I. Erlich, "Assessment and enhancement of small signal stability considering uncertainties," *Power Systems, IEEE Transactions on*, vol. 24, no. 1, pp. 198–207, 2009.

[4] R. Preece, K. Huang, and J. Milanovic, "Probabilistic small-disturbance stability assessment of uncertain power systems using efficient estimation methods," *Power Systems, IEEE Transactions on*, vol. 29, no. 5, pp. 2509–2517, Sept 2014.

[5] I. A. Hiskens and J. Alseddiqui, "Sensitivity, approximation, and uncertainty in power system dynamic simulation," *Power Systems, IEEE Transactions on*, vol. 21, no. 4, pp. 1808–1820, 2006.

[6] A. Chakrabortty and E. Scholtz, "Time-scale separation designs for performance recovery of power systems with unknown parameters and faults," *Control Systems Technology, IEEE Transactions on*, vol. 19, no. 2, pp. 382–390, 2011.

[7] C. L. DeMarco, V. Balakrishnan, and S. Boyd, "A branch and bound methodology for matrix polytope stability problems arising in power systems," in *Decision and Control, 1990., Proceedings of the 29th IEEE Conference on*. IEEE, 1990, pp. 3022–3027.

[8] K. M. Son and J. K. Park, "On the robust lqg control of tcsc for damping power system oscillations," *Power Systems, IEEE Transactions on*, vol. 15, no. 4, pp. 1306–1312, 2000.

[9] B. Pal and B. Chaudhuri, *Robust control in power systems*. Springer Science & Business Media, 2006.

[10] R. A. Jabr, B. C. Pal, and N. Martins, "A sequential conic programming approach for the coordinated and robust design of power system stabilizers," *Power Systems, IEEE Transactions on*, vol. 25, no. 3, pp. 1627–1637, 2010.

[11] H. Bevrani, *Robust power system frequency control*. Springer, 2009, vol. 85.

[12] M. ApS, *The MOSEK optimization toolbox for MATLAB manual. Version 7.1 (Revision 28).*, 2015. [Online]. Available: http://docs.mosek.com/7.1/toolbox/index.html

[13] T. L. Vu and K. Turitsyn, "Lyapunov functions family approach to transient stability assessment," *arXiv preprint arXiv:1409.1889*, 2014.

[14] M. Anghel, J. Anderson, and A. Papachristodoulou, "Stability analysis of power systems using network decomposition and local gain analysis," in *Bulk Power System Dynamics and Control-IX Optimization, Security and Control of the Emerging Power Grid (IREP), 2013 IREP Symposium*. IEEE, 2013, pp. 1–7.

[15] P. Gahinet, A. Nemirovskii, A. J. Laub, and M. Chilali, "The lmi control toolbox user's guide," 1995.

[16] H.-S. Wang, *H-infinity Control for Nonlinear Descriptor Systems*. Springer Science & Business Media, 2006, vol. 326.

[17] S. P. Boyd, L. El Ghaoui, E. Feron, and V. Balakrishnan, *Linear matrix inequalities in system and control theory*. SIAM, 1994, vol. 15.

[18] J. Lofberg, "Yalmip: A toolbox for modeling and optimization in matlab," in *Computer Aided Control Systems Design, 2004 IEEE International Symposium on*. IEEE, 2004, pp. 284–289.

[19] E. Davison and E. Kurak, "A computational method for determining quadratic lyapunov functions for non-linear systems," *Automatica*, vol. 7, no. 5, pp. 627–636, 1971.

[20] A. Tesi, F. Villoresi, and R. Genesio, "On the stability domain estimation via a quadratic lyapunov function: convexity and optimality properties for polynomial systems," *Automatic Control, IEEE Transactions on*, vol. 41, no. 11, pp. 1650–1657, 1996.

[21] G. Chesi, A. Garulli, A. Tesi, and A. Vicino, "Lmi-based computation of optimal quadratic lyapunov functions for odd polynomial systems," *International Journal of Robust and Nonlinear Control*, vol. 15, no. 1, pp. 35–49, 2005.

[22] W. Tan and A. Packard, "Stability region analysis using polynomial and composite polynomial lyapunov functions and sum-of-squares programming," *Automatic Control, IEEE Transactions on*, vol. 53, no. 2, pp. 565–571, 2008.

[23] B. R. Barmish, "Necessary and sufficient conditions for quadratic stabilizability of an uncertain system," *Journal of Optimization theory and applications*, vol. 46, no. 4, pp. 399–408, 1985.

[24] V. Balakrishnan, S. Boyd, and S. Balemi, "Branch and bound algorithm for computing the minimum stability degree of parameter-dependent linear systems," *International Journal of Robust and Nonlinear Control*, vol. 1, no. 4, pp. 295–317, 1991.

[25] K. Wang, A. N. Michel, and D. Liu, "Necessary and sufficient conditions for the hurwitz and schur stability of interval matrices," *Automatic Control, IEEE Transactions on*, vol. 39, no. 6, pp. 1251–1255, 1994.

[26] P. Kundur, N. Balu, and M. Lauby, *Power system stability and control*, 1994.

[27] Abb generators for diesel and gas engines. Technical Specifications for type designation AMG-0200CC04 (60kVA) and AMG-0180BB04 (25kVA). [Online]. Available: http://new.abb.com/motors-generators/generators/generators-for-diesel-and-gas-engines/low-voltage-generators-for-industrial-applications

[28] D. Lee, D. Baker, K. Bess *et al.*, "Ieee recommended practice for excitation system models for power system stability studies," *Energy development and power generation committee of power engineering society*, 2005.

[29] K. Yeager and J. Willis, "Modeling of emergency diesel generators in an 800 megawatt nuclear power plant," *Energy Conversion, IEEE Transactions on*, vol. 8, no. 3, pp. 433–441, 1993.

[30] A. Kasem Alaboudy, H. Zeineldin, and J. L. Kirtley, "Microgrid stability characterization subsequent to fault-triggered islanding incidents," *Power Delivery, IEEE Transactions on*, vol. 27, no. 2, pp. 658–669, 2012.

[31] F. Katiraei and M. R. Iravani, "Power management strategies for a microgrid with multiple distributed generation units," *Power Systems, IEEE Transactions on*, vol. 21, no. 4, pp. 1821–1831, 2006.

[32] L. Vandenberghe, V. R. Balakrishnan, R. Wallin, and A. Hansson, "On the implementation of primal-dual interior-point methods for semidefinite programming problems derived from the kyp lemma," in *Conference on Decision and Control*. Citeseer, 2003, pp. 4658–4663.

[33] M. S. Andersen, L. Vandenberghe, and J. Dahl, "Linear matrix inequalities with chordal sparsity patterns and applications to robust quadratic optimization," in *Computer-Aided Control System Design (CACSD), 2010 IEEE International Symposium on*. IEEE, 2010, pp. 7–12.